05

Abnormal electrical resistivity of Co−Fe−Si−B−Nb−R alloys in amorphous and crystalline states

© V.E. Sidorov,[1,2] B.A. Rusanov,[1] S.A. Petrova,[2,3] L.D. Son,[1,2,3] V.I. Lad'yanov[4]

[1] Ural State Pedagogical University, Ekaterinburg, Russia
[2] Ural Federal University after the first President of Russia B.N. Yeltsin, Yekaterinburg, Russia
[3] Institute of Metallurgy of Ural Branch of the Russian Academy of Science, Ekaterinburg, Russia
[4] Udmurt Federal Research Center, Ural Branch Russian Academy of Sciences, Izhevsk, Russia
e-mail: rusfive@mail.ru

Received July 29, 2022
Revised October 6, 2022
Accepted October 10, 2022

Electrical resistivity of $Co_{48}Fe_{25}Si_4B_{19}Nb_4$ amorphous alloy and with small additions of rare-earth metals (= Nd, Sm, Tb, Yb) was studied using the AC four-probe method. It was found that these alloys have a specific behavior of electrical resistivity after crystallization-temperature dependences of resistivity at cooling are non-linear and can be fitted as $\ln R \sim T^{-1/4}$.

Keywords: amorphous alloys, metallic glasses, electrical resistivity, rare-earth metals.

DOI: 10.21883/TP.2023.01.55540.195-22

Introduction

Bulk metallic glasses (BMG) and amorphous ribbons based on cobalt and iron, especially Co−Fe−Si−B−Nb compositions, are objects with unique mechanical, magnetic, and electrical properties [1–3]. These materials have already found industrial application. In particular, Co- and Fe-based amorphous rods and ribbons are used as new highly sensitive sensors [4–6].

Cobalt-based BMGs have excellent soft magnetic properties: their saturation magnetization can be as high as 1.1 T at a coercive force of $H_c = 0.7$ A/m; the same alloys in crystalline state have $B_{\max} = 0.2$ T at $H_c > 1000$ A/m. In addition, these BMGs are characterized by ultrahigh values of fracture resistance at a level of 4250−4450 MPa and plastic deformation of 0.6−1.3% (for crystalline analogs, these parameters are 4−5 times lower) [7,8].

However, the wide application of cobalt-based amorphous materials is limited, firstly, by the difficulty of obtaining and, secondly, by the instability of amorphous state, which can crystallize under certain external influences. Therefore, the influence of various small additions on the glass-forming ability (GFA) and properties of these alloys is of special interest for researchers, because doping is the main technological practice to produce BMG. Previously we studied the effect of gallium, tin and antimony on GFA of CoFeSiBNb alloys. All these elements completely meet the criteria formulated by A. Inoue, however, only gallium results in increase in the glass-forming ability of the alloys [9,10].

In this study we have focused on the specific electrical resistivity of the $Co_{48}Fe_{25}Si_4B_{19}Nb_4$ alloy (the base composition) and the same alloy with small additions of rare-earth metals (REM) (Nd, Sm, Tb, Yb). The base composition is characterized by a high Curie temperature, which makes it promising for practical applications. It was turned out that the alloys crystallized from bulk amorphous state demonstrate very unusual temperature dependence of electrical resistivity during cooling.

1. Materials and experimental techniques

The $Co_{48}Fe_{25}Si_4B_{19}Nb_4$ base composition alloys and alloys with additions of 1 and 2 at.% of REMs (Nd, Sm, Tb, Yb) were produced by remelting of pure components in an induction furnace at 1700 K for 30 min in argon atmosphere.

BMGs in the form of rods (with a diameter of 2 mm, a height of 18−20 mm) were produced by the method of vacuum suction of the melt into a water-cooled copper mold. To facilitate resistivity measurements, the samples were also obtained in the form of ribbons (wide 3−5 mm, thickness 40−45 μm) by planar flow casting method in a controlled argon atmosphere after heating the melts to 1500−1523 K in an induction furnace and injecting them onto rotating water-cooled copper wheel.

Structure of the samples was analyzed by X-ray diffraction using a Bruker D8 Advance (CuK_α-radiation, 40 kV and 35 mA) diffractometer in the parallel beam configuration. At the primary beam a Goebel mirror was installed, while a Soller slit 0.23° and a LiF-monochromator were installed at the reflected beam. Measurements were performed with a constant incident angle of 10°, in an angle range of 20−105°, with a step of $\Delta 2\theta = 0.05°$. Typical time of data collection per one step was 6 s, while signal-to-noise ratio in the region of the main diffusion maximum was not lower than 5. Electrical resistivity of amorphous ribbons was measured by AC four-probe method (distance between probes — 30 mm) under protective argon atmosphere at

continuous heating/cooling rates of 10 K/min. For a detailed description of the measurement method, please refer to [11]. Crystallization process of amorphous alloys was studied using differential thermal analysis on a PerkinElmer DTA-7 setup at a heating rate of 10 K/min for checking amorphous-crystalline transition. The instrument was pre-calibrated by melting temperatures of pure aluminum and gold.

The distribution of surface electric potentials was studied by Kelvin Probe Microscopy technique using NT-MDT Solver Next atomic force microscope. The two-pass measurement scheme was used, when in the first pass, surface topography of the scan line was measured in the Semicontact Mode, then the probe was lifted above the surface to the height dZ and thus moved over the surface following the topography contour.

2. Results and discussion

All the samples produced with fast quenching appeared to be X-ray amorphous.

Electrical resistivity temperature dependence for $Co_{48}Fe_{25}Si_4B_{19}Nb_4$ alloy is shown in Fig. 1. The following features are worth noting.

Specific electrical resistivity R of the base composition in amorphous state has nearly zero temperature coefficient (TCR), although all the samples are ferromagnetic materials (according to the results of magnetic susceptibility measurements the Curie temperature of these alloys is about 1080 K). This result may be indicative of the fact that absolute values of R are quite high (at a level of $120-140\,\mu\Omega\,\text{cm}$) and are mainly defined by the short-range order in the alloy. Above $T \approx 550$ K an insignificant increase in resistivity was recorded.

For detailed consideration of resistivity behavior during crystallization, Fig. 2 shows the DTA and resistivity curves in the same temperature coordinates.

It is found that during crystallization, the growth of resistivity begins on 15–20 K higher than the onset of crystallization (T_X). This fact can indicate that the growing new phase and its boundaries must reach a certain size to contribute to electrical resistivity.

The R(T) curves for alloys containing rare-earth additions are shown in Figure 3 For alloys with 2 at.% REM, the dependences are similar to the presented ones and are not shown to save the space.

It is found that the lowest $R(T)$ values are demonstrated by the alloy with1 at.% addition of terbium (a rare-earth metal from the middle of the lanthanide series). Among the alloys with 2 at.% REM, the lowest $R(T)$ values correspond to the alloy with samarium.

The R(T) curves obtained at cooling were found to be smooth for all investigated compositions. This is indicative of the absence of phase transformations in alloys at cooling down to the room temperature. All phases formed as a result of the crystallization from amorphous state were remained down to the room temperature. We made X-ray

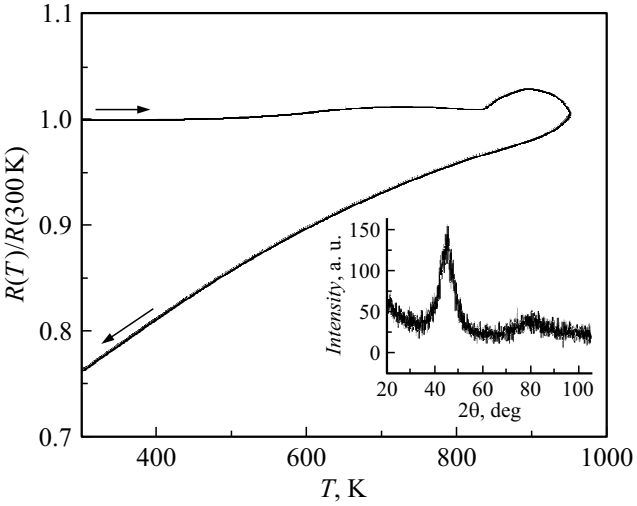

Figure 1. Temperature dependence of relative electrical resistivity of the $Co_{48}Fe_{25}Si_4B_{19}Nb_4$ amorphous alloy (the base composition). In the insert — X-ray diffraction pattern of the metal ribbon.

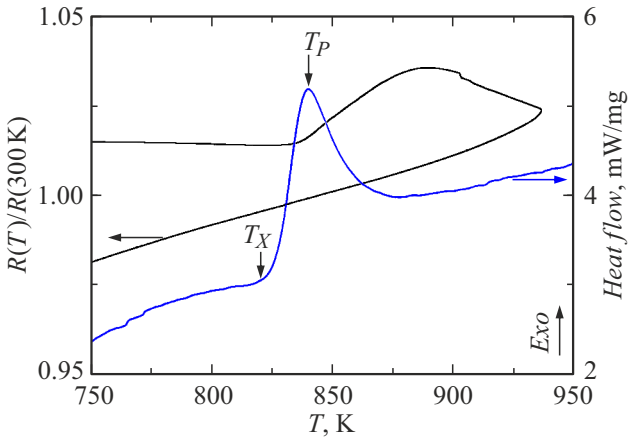

Figure 2. Temperature dependence of relative electrical resistivity and DTA-curve of the amorphous $Co_{48}Fe_{25}Si_4B_{19}Nb_4$ ribbon at a heating rate of 10 K/min.

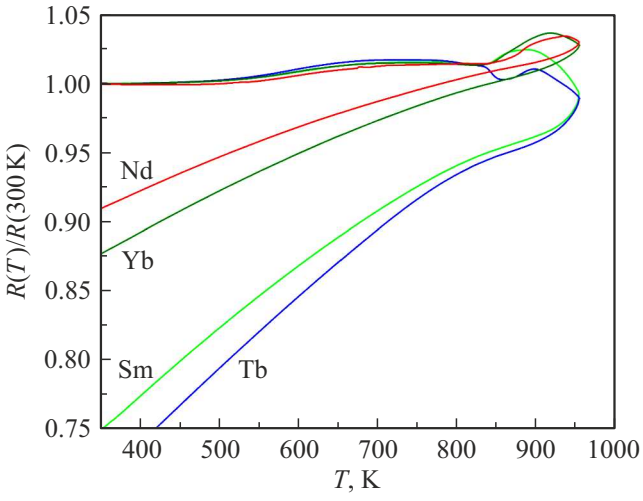

Figure 3. Temperature dependencies of relative electrical resistivity of amorphous $Co_{48}Fe_{25}Si_4B_{19}Nb_4$–1 at.% REM alloys.

phase analysis of the samples after resistivity experiments. The phase composition of crystallized samples was as follows (for the base composition):

1) pure Co and solution of Co–Fe (microareas with different concentration) — 55%;

2) different oxides ($Fe_{2.2}Co_{0.8}O_4$ and CoO) — 23%;

3) complex ($Fe_3Co_3B_2$, $Fe_3Si_{0.4}B_{0.6}$) and simple (Co_2B, Fe_2B) borides — 15%;

4) metastable phase 23 : 6 ($Co_{11.2}Fe_{9.8}Nb_2B4_6$) — 7%.

Moreover, the X-ray diffraction pattern shows traces of quartz (less than 1%), which can indicate the interaction between the melt and the crucible at casting. The presence of oxides is also quite natural, because electrical resistivity measurements were carried out in an argon flow without evacuating the sample. It is found that the addition of rare-earth metals increases the quantity of Co–Fe phase (about 65%), while the quantity of oxides and borides decreases (20 and 4%, respectively). It is the most likely that REM atoms form the REM_5Si_3 compound and partly transit to the 23 : 6 phase, which quantity increases as well.

The most interesting was the form of $R(T)$ temperature dependences during cooling. Resistivity increases with temperature growth, which is indicative of the presence of free electrons, i.e. the metal type of conductivity. However, the temperature dependence is not a power-function! By plotting the graph of $\ln R(T^{-1/4})$ (Fig. 4), we can see, that the dependencies of

$$\ln\left(\frac{R}{R_0}\right) \sim T^{-\frac{1}{4}} \qquad (1)$$

become linear with a confidence probability of 0.99, i.e. this conclusion is substantially true. Note, that dependence (1) is valid in relation to all added REMs and observed for all investigated samples.

Dependence (1) can not arise in a bulk solid metal sample, because in this case Kubo–Greenwood formulation for the specific electrical resistivity is valid (see, for example, [12]), which can only yield a power -function dependence. A dependence similar to (1) was observed for nanocomposite samples in [13], except for the significant fact that the proportionality factor between $\ln(R)$ and $T^{-1/4}$ was negative, i.e. the specific electrical resistivity decreased with temperature growth.

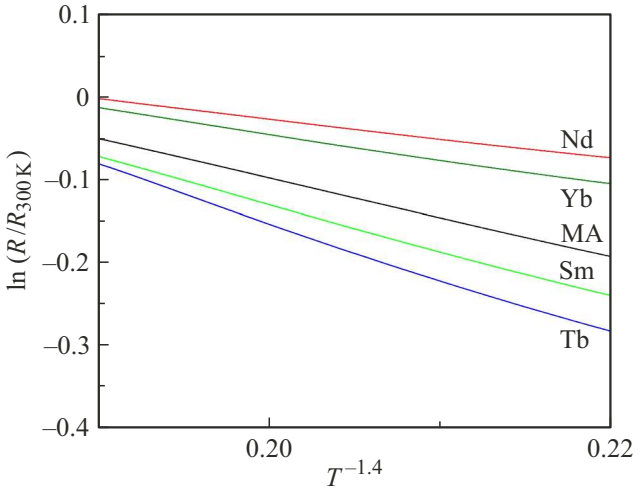

Figure 4. Dependence of $\ln(R/R_{300K})$ on $T^{-1/4}$ for CoFeSiBNb–1 at.% REM alloys.

In this case, the conductivity is hopping with a variable hop length (the so-called Mott conductivity, see [12]) for electrons localized in nanocomposite grains. In our case, the conductivity is provided by free electrons, and the temperature dependence (1) can arise due to the specific spatial structure of the conductive region, which leads to the activation mechanism of electron scattering. Let the metal phase be a percolation cluster consisting of some structural units with a wide range of sizes. In general, the scattering probability in a structural unit of r size is defined by the following two factors:

$$w(r) \sim \exp\left(-\alpha\frac{r}{2\lambda_F}\right)\exp\left(-\beta\frac{1}{2Tr^3N(E_F)}\right). \qquad (2)$$

The first factor, $\sim \exp\left(-\alpha\frac{r}{2\lambda_F}\right)$ is the probability of collision when passing through a globule of r size (λ_F — Fermi wavelength, α — a coefficient describing the metal). The second factor, $\sim \exp\left(-\beta\frac{1}{2Tr^3N(E_F)}\right)$ is the probability to get energy for localization in the globule volume as a result of collision (here $N(E_F)$ — density of states at Fermi energy, a β — a coefficient describing the metal).

Resistivity is proportional to the average scattering probability:

$$R \sim \int dr\, w^2(r). \qquad (3)$$

The integration in (3) is performed over the total range of sizes r. If it is wide enough, then the integral (3) can be estimated by the saddle-point method (see, for example, [14]), so that

$$R(T) \sim \exp\left(\frac{A}{T^{1/4}}\right), \quad A = \sqrt[4]{\frac{\alpha^3\beta}{\lambda_F^3 N(E_F)}}\left(\sqrt[4]{3}+1\right). \qquad (4)$$

It should be stressed that this dependence is obtained in accordance with the assumption that the metal phase is a percolation cluster composed of compact structural units with a wide range of sizes.

For the investigated alloys this can mean that non-conducting oxides and borides formed in the process of crystallization build up a thin extensive network that penetrates the entire volume of the sample. Therefore, the transition of electrons from one conducting microregion to another occurs in tunneling mode. The fact that conductive microregions are rather small and separated by nonconductive layers is confirmed by the results of atomic force microscopy (Fig. 5).

This type of electrical resistivity temperature dependence for metallic alloys was discovered by us for the first time. Previously, such dependence of conductivity was

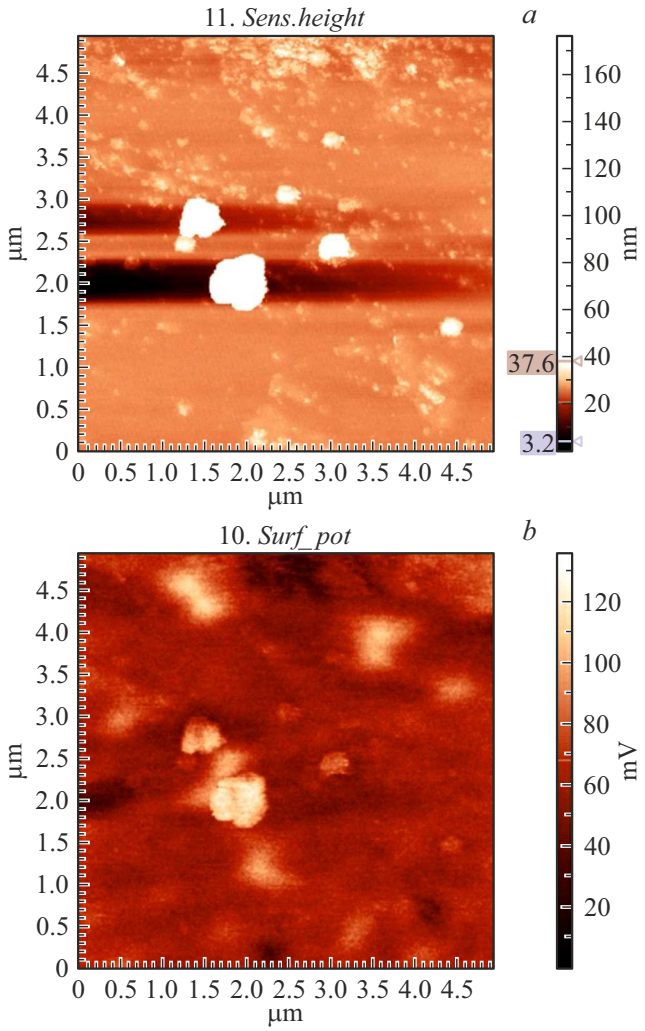

Figure 5. Surface topography (a) and spatial distribution of potential (b) for the $Co_{48}Fe_{25}Si_4B_{19}Nb_4$ – 2 at.% Sm alloy.

experimentally observed only in a narrow range at low temperatures for Co-based granular structures (see [15,16] and Ref. therein).

Conclusion

It is shown for the first time that temperature dependencies of electrical resistivity of alloys based on the Co–Fe–Si–B–Nb system follow the law of 1/4, i.e. $\ln R \sim T^{-1/4}$, in the process of cooling. This fact means that non-conducting oxides and borides arising during crystallization form a thin branched network that permeates the entire volume of the sample. Consequently, transition of electrons from one conducting microarea to another occurs in tunneling mode. This fact must be taken into consideration when manufacturing products for the industrial electronics.

Conflict of interest

The authors declare that they have no conflict of interest.

References

[1] C. Suryanarayana, A. Inoue. *Bulk Metallic Glasses* (CRC Press, 2020), 542 p.
[2] G. Abrosimova, N. Volkov, V. Chirkova, A. Aronin. Mater. Lett., **297**, 129996 (2021). DOI: 10.1016/j.matlet.2021.129996
[3] G.E. Abrosimova, N.A. Volkov, E.A. Pershina, V.V. Chirkova, I.A. Sholin, A.S. Aronin. J. Non-Cryst. Solids, **565**, 120864 (2021). DOI: 10.1016/j.jnoncrysol.2021.120864
[4] K. Mohri, K. Kawashima, T. Kozhawa, Y. Yoshida, L.V. Panina. IEEE Tr. Magn., **28**, 3150 (1992). DOI: 10.1109/20.179741
[5] L.V. Panina, K. Mohri, T. Uchiyama, M. Noda, K. Bushida. IEEE Tr. Magn., **31**, 1249 (1995). DOI: 10.1109/20.364815
[6] H.Q. Guo, H. Kronmuller, T. Dragon, Z.H. Cheng, B.G. Shen. J. Appl. Phys., **89**, 514 (2001). DOI: 10.1063/1.1331649
[7] Q. Man, H. Sun, Y. Dong, B. Shen, H. Kimura, A. Makino, A. Inoue. Intermetallics, **18** (10), 1876 (2010). DOI: 10.1016/j.intermet.2010.02.047
[8] Y. Dong, A. Wang, Q. Man, B. Shen. Intermetallics, **23**, 63 (2012). DOI: 10.1016/j.intermet.2011.12.020
[9] V. Sidorov, J. Hosko, V. Mikhailov, I. Rozkov, N. Uporova, P. Svec, D. Janickovic, I. Matko, P. Svec Sr, L. Malyshev. J. Magn. Magn. Mater., **354**, 35 (2014). DOI: 10.1016/j.jmmm.2013.10.038
[10] V.E. Sidorov, V.A. Mikhailov, A.A. Sabirzyanov. Russ. Metall., **2**, 109 (2016). DOI: 10.1134/S0036029516020166
[11] V. Sidorov, P. Svec, D. Janickovic, V. Mikhailov, L. Son. J. Magn. Magn. Mater., **395**, 324 (2015). DOI: 10.1016/j.jmmm.2015.07.072
[12] N.F. Mott, E.A. Davis. *Electron Processes in Non-Crystalline Materials* (Clarendon Press, Oxford, 1979), 590 p.
[13] S.A. Gridnev, Yu.E. Kalinin, A.V. Sitnikov, O.V. Stogney. *Nelineynye yavleniya v nano- i mikrogeterogennykh sistemakh* (Laboratoriya znaniy, M., 2020), 355 p. (in Russian).
[14] C.M. Bender, S.A. Orszag. *Advanced Mathematical Methods for Scientists and Engineers* (Springer, NY., 1999), 593 p.
[15] Y.E. Kalinin, A.N. Remizov, A.V. Sitnikov. Phys. Solid State, **46**, 2146 (2004). DOI: 10.1134/1.1825563
[16] I.V. Zolotukhin, Yu.E. Kalinin, A.T. Ponomarenko, V.G. Shevchenko, A.V. Sitnikov, O.V. Stognei, O. Figovsky. J. Nanostructured Polym. Nanocomposites, **2** (1), 23 (2006).